

Discrete Fractional Fourier Transform Based on Orthogonal Projections

Soo-Chang Pei, *Senior Member, IEEE*, Min-Hung Yeh, and Chien-Cheng Tseng, *Member, IEEE*

Abstract—The continuous fractional Fourier transform (FRFT) performs a spectrum rotation of signal in the time–frequency plane, and it becomes an important tool for time-varying signal analysis. A discrete fractional Fourier transform has been recently developed by Santhanam and McClellan, but its results do not match those of the corresponding continuous fractional Fourier transforms. In this paper, we propose a new *discrete fractional Fourier transform* (DFRFT). The new DFRFT has DFT Hermite eigenvectors and retains the eigenvalue-eigenfunction relation as a continuous FRFT. To obtain DFT Hermite eigenvectors, two orthogonal projection methods are introduced. Thus, the new DFRFT will provide similar transform and rotational properties as those of continuous fractional Fourier transforms. Moreover, the relationship between FRFT and the proposed DFRFT has been established in the same way as the conventional DFT-to-continuous-Fourier transform.

Index Terms—Discrete Fourier transform, discrete fractional Fourier transform, Fourier transform, fractional Fourier transform.

I. INTRODUCTION

THE FOURIER transform (FT) is one of the most frequently used tools in signal analysis [1]. A generalization of the Fourier transform—the fractional Fourier transform (FRFT)—has been proposed in [2] and [3] and has become a powerful tool for time-varying signal analysis. In time-varying signal analysis, it is customary to use the time–frequency plane, with two orthogonal time and frequency axes [4]. Because the successive two forward Fourier transform operations will result in the reflected version of the original signal, the FT can be interpreted as a rotation of signal by the angle $\pi/2$ in the time–frequency plane and represented as an orthogonal signal representation for sinusoidal signal. The FRFT performs a rotation of signal in the continuous time–frequency plane to any angle and serves as an orthonormal signal representation for the chirp signal. The fractional Fourier transform is also called *rotational Fourier transform* or *angular Fourier transform* in some documents. Besides being a generalization of the FT, the

FRFT has been proved to relate to other time-varying signal analysis tools, such as Wigner distribution [4], short-time Fourier transform [4], wavelet transform, and so on. The applications of the FRFT include solving differential equations [2], quantum mechanics [3], optical signal processing [5], time-variant filtering and multiplexing [5]–[8], swept-frequency filters [9], pattern recognition [10], and time–frequency signal analysis [11]–[13]. Several properties of the FRFT in signal analysis have been summarized in [9].

Many methods for realizing the FRFT have been developed, but most of them are to utilize the optical implementation [14], [15] or numerical integration. Because the FRFT is a potentially useful tool for signal processing, the direct computation of the fractional Fourier transform in digital computers has become an important issue. The ideal discrete fractional Fourier transform (DFRFT) will be a generalization of the discrete Fourier transform (DFT) that obeys the rotation rules as the continuous FRFT and provides similar results as the FRFT. In [16], a method for a numerical integration FRFT has been proposed, but the method does not obey the rotation rules, and the signal cannot be recovered from its inverse transform. In [17], Santhanam and McClellan have developed a discrete FRFT, but their method does not provide the same transforms to match those of the continuous case. In this paper, we present a new *discrete fractional Fourier transform* (DFRFT). This DFRFT is a generalization of the DFT and will provide similar transforms as those of the continuous case. The relationship between the DFRFT and the FRFT can also be established and discussed in detail. Moreover, the proposed DFRFT has important unitary and rotation properties.

This paper is organized as follows. In Section II, the previous development of continuous and discrete fractional Fourier transforms are reviewed. The concept for developing the DFRFT to have similar results as the continuous corresponding case are described in Section III. Two acceptable solutions for the DFRFT are considered and proposed in Section III. Then, the relationships between the FRFT and the DFRFT can be established in Section IV. Finally, conclusions and discussions are made in Section V.

II. PRELIMINARY

A. Continuous FRFT

The Fourier transform of a signal can be interpreted as a $\pi/2$ angle rotation of the signal in the time–frequency plane. The FRFT is then developed and treated as a rotation of signal

Manuscript received December 2, 1996; revised February 19, 1998. This work was supported by the National Science Council, R.O.C., under Contract NSC 85-2213-E002-025. The associate editor coordinating the review of this paper and approving it for publication was Dr. Akram Aldroubi.

S.-C. Pei is with the Department of Electrical Engineering, National Taiwan University, Taipei, Taiwan, R.O.C. (e-mail: pei@cc.ee.ntu.edu.tw).

M.-H. Yeh is with the Department of Computer Information Science, Tamsui Oxford University College, Tamsui, Taipei, Taiwan, R.O.C.

C.-C. Tseng was with the Department of Electronics Engineering, Hwa Hsia College of Technology and Commerce, Taipei, Taiwan, R.O.C. He is now with the Department of Computer and Communication Engineering, National Kaohsiung First University of Science and Technology, Taipei, Taiwan, R.O.C.

Publisher Item Identifier S 1053-587X(99)03244-4.

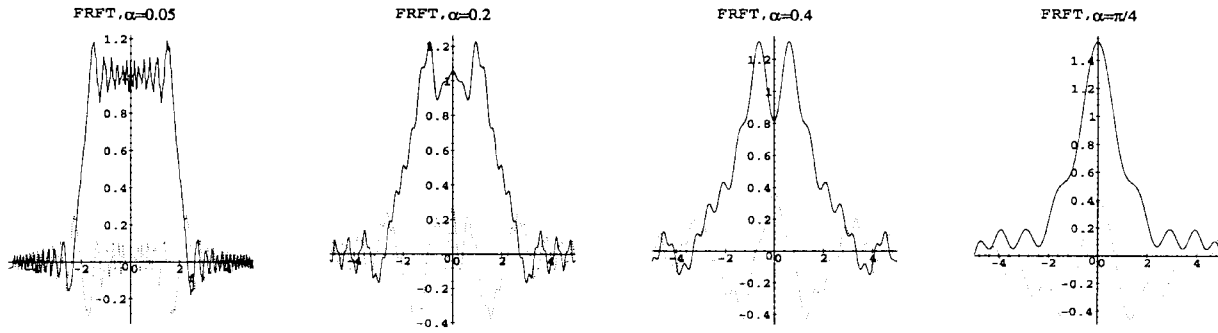


Fig. 1. Fractional Fourier transform of a rectangular window. $x(t) = 1$ when $-2 \leq t \leq 2$, and $x(t) = 0$ otherwise. Real part: solid line. Imaginary part: dashed line.

to any angles in the time–frequency plane [9]. The transform kernel of continuous FRFT is defined as [2], [3], [6], [9]

$$K_{\alpha}(t, u) = \begin{cases} \sqrt{\frac{1-j \cot \alpha}{2\pi}} \exp\left(j\left(\frac{t^2+u^2}{2}\right) \cot \alpha - jut \csc \alpha\right) & \text{if } \alpha \text{ is not a multiple of } \pi \\ \delta(t-u) & \text{if } \alpha \text{ is a multiple of } 2\pi \\ \delta(t+u) & \text{if } \alpha + \pi \text{ is a multiple of } 2\pi \end{cases} \quad (1)$$

$$= \sum_{n=0}^{\infty} e^{-jn\alpha} H_n(t) H_n(u). \quad (2)$$

where α indicates the rotation angle of transformed signal for the FRFT. $H_n(t)$ is the n th-order normalized Hermite function with unit variance. The n th-order normalized Hermite function with variance σ is defined as

$$H_{\sigma, n}(t) = \frac{1}{(2^n n! \sqrt{\pi} \sigma)^{1/2}} h_n\left(\frac{t}{\sigma}\right) e^{-(t^2/2\sigma^2)} \quad (3)$$

where $h_n(\cdot)$ is the n th-order Hermite polynomial [18]. Because the normalized Hermite function with unitary variance, $H_n(\cdot)$ is the eigenfunction of the FRFT, (2) provides an eigendecomposition representation of the FRFT kernel. The equivalence of (1) and (2) has been proved in [3]. Using the kernel of the FRFT, the FRFT of the signal $x(t)$ by angle α is computed as

$$\mathcal{X}_{\alpha}(u) = \int_{-\infty}^{\infty} x(t) K_{\alpha}(t, u) dt \quad (4)$$

$$= \sum_{n=0}^{\infty} H_n(u) \left(e^{-jn\alpha} \int_{-\infty}^{\infty} x(t) H_n(t) dt \right). \quad (5)$$

Equation (5) indicates that the FRFT can be interpreted as a weighting summation of Hermite functions. The weighting coefficients are obtained from multiplying the phase term $e^{-jn\alpha}$ and the inner product of the input signal and the corresponding Hermite function. In [19], a rotation operation using Hermite functions has also been proposed, and the rotation output of the signal is also the weighting summation of Hermite functions. However, the Hermite functions in [19] with a different scaling to those of the FRFT. Thus, it will have a different phase term in the weighting coefficients.

Fig. 1 shows the FRFT of the rectangular window function [$x(t) = 1$ for $|t| \leq 2$; and $x(t) = 0$, elsewhere] for various angles. The real parts of the FRFT or DFRFT in this paper are plotted by solid lines, and the imaginary parts of the FRFT or DFRFT are indicated by dashed lines.

B. The Old DFRFT

The kernel matrix of the DFRFT is obtained by computing the fractional power for the DFT kernel matrix. The fractional power of the DFT kernel matrix and the rotation angles in the DFRFT essentially mean the same thing. In order to avoid ambiguity, the Greek subscripts (for example, α and β) are used to denote the rotation angles in the time–frequency plane, and the English superscripts are used to denote the fractional power values of the DFT kernel matrices in this paper. The conventional methods to compute the DFRFT in [17] and [20] are mainly on numerical computing the fractional power of the DFT kernel matrix. The fractional power of the DFT kernel matrix [20] is calculated by (6)

$$\mathbf{F}^t = a_0(t)\mathbf{F}^0 + a_1(t)\mathbf{F}^1 + a_2(t)\mathbf{F}^2 + a_3(t)\mathbf{F}^3 \quad (6)$$

where

$$a_i(t) = \frac{1}{4} \sum_{k=1}^4 e^{j(\pi/2)(t-i)k}. \quad (7)$$

Applying the above defined kernel to the signal $\mathbf{x}(n)$, the DFRFT of the signal $\mathbf{x}(n)$ is computed as

$$\mathbf{F}^t[\mathbf{x}(n)] = a_0(t)\mathbf{x}(n) + a_2(t)\mathbf{x}(-n) + a_1(t)\mathbf{X}(n) + a_3(t)\mathbf{X}(-n) \quad (8)$$

where $\mathbf{X}(n)$ is the conventional DFT of signal $\mathbf{x}(n)$. Equation (8) indicates that the DFRFT of the signal $\mathbf{x}(n)$ is the linear combination of the four major angular parts: the original signal $\mathbf{x}(n)$, its DFT $\mathbf{X}(n)$, a circular reflected version of the signal $\mathbf{x}(n)$ ($\mathbf{x}(-n)$), and a circular reflected version of its DFT $\mathbf{X}(-n)$.

Fig. 2 shows the results of this DFRFT produced by a discrete rectangular window. The rectangular window used here is defined as [$N = 73$, $f(k) = 1$, $-6 \leq k \leq 6$; otherwise $f(k) = 0$]. The discrete results shown in Fig. 2 are quite different from the results of Fig. 1. Furthermore, the middle transform result for $\alpha = 0.4$ is not the intermediate state of the two results $\alpha = 0.2$ and $\alpha = \pi/4$.

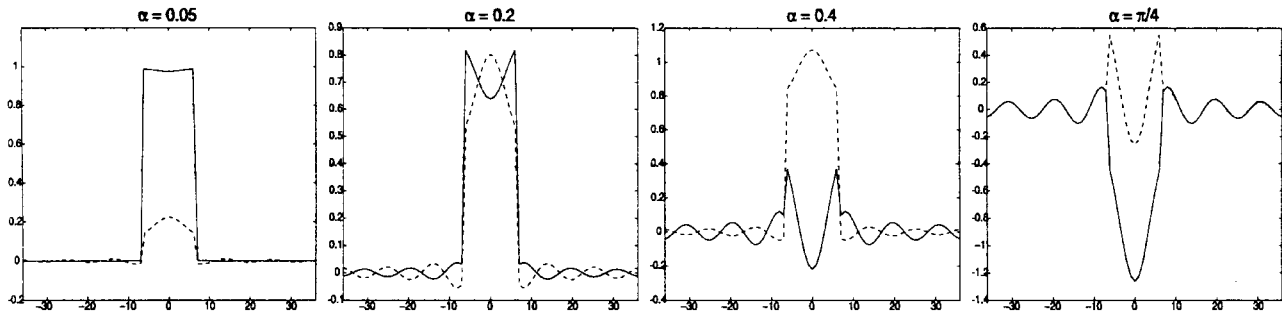


Fig. 2. Old DFRFT of a rectangular window function. $x(n) = 1$ when $-6 \leq n \leq 6$, and $x(n) = 0$ otherwise. The output is quite different from the continuous FRFT in Fig. 1.

TABLE I
MULTIPLICITIES OF THE EIGENVALUES OF DFT KERNEL MATRIX

| N | $\sharp(N, 0)$ Multiplicity of 1 | $\sharp(N, 1)$ Multiplicity of $-j$ | $\sharp(N, 2)$ Multiplicity of -1 | $\sharp(N, 3)$ Multiplicity of j |
|----------|--|---|---|--|
| $4m$ | $m + 1$ | m | m | $m - 1$ |
| $4m + 1$ | $m + 1$ | m | m | m |
| $4m + 2$ | $m + 1$ | m | $m + 1$ | m |
| $4m + 3$ | $m + 1$ | $m + 1$ | $m + 1$ | m |

III. DEVELOPMENT OF DFRFT

A. Eigendecomposition of DFRFT

The development of our DFRFT is based on the eigendecomposition of the DFT kernel, and many properties of the DFT matrix eigenvalues and eigenvectors have been discussed in [20] and [21]. Here, we only summarize some results for our further development of DFRFT.

Proposition 1: The eigenvalues of \mathbf{F} are $\{1, -j, -1, j\}$, and its multiplicities are shown in Table I.

Proof: See [21].

In Table I, a multiplicity function $\sharp(N, k)$ is defined. This function is used to denote the DFT eigenvalue multiplicity for N . The parameter k is the index for the DFT eigenvalue $e^{-j(\pi/2)^k}$. The eigenvectors of the DFT matrix constitute four major eigensubspaces— E_0 , E_1 , E_2 , and E_3 —and each is corresponding to one of the four eigenvalues— 1 , $-j$, -1 , and j —respectively. The eigenvalue multiplicities of DFT matrix indicate the ranks of the DFT eigensubspaces [21], [22].

In [22], a method for computing the DFT eigenvectors has been introduced, but it cannot obtain the real-valued DFT eigenvectors. In [20], a novel matrix \mathbf{S} is introduced to compute the real and complete set of DFT eigenvectors very elegantly.

Proposition 2: A matrix \mathbf{S} can be used to compute the real eigenvectors of the DFT matrix \mathbf{F} , and matrix \mathbf{S} is defined as

$$\mathbf{S} = \begin{bmatrix} 2 & 1 & 0 & 0 & \cdots & 1 \\ 1 & 2 \cos \omega & 1 & 0 & \cdots & 0 \\ 0 & 1 & 2 \cos 2\omega & 1 & \cdots & 0 \\ \vdots & \vdots & \vdots & \ddots & \ddots & \vdots \\ 1 & 0 & 0 & 0 & \cdots & 2 \cos(N-1)\omega \end{bmatrix} \quad (9)$$

where $\omega = 2\pi/N$. Matrix \mathbf{S} commutes with the DFT kernel matrix \mathbf{F} , and then, it satisfies the commutative property

$$\mathbf{S}\mathbf{F} = \mathbf{F}\mathbf{S}. \quad (10)$$

The eigenvectors of matrix \mathbf{S} will also be the eigenvectors of the DFT kernel matrix \mathbf{F} , but they correspond to different eigenvalues.

Proof: See [20].

B. DFT Hermite Eigenvectors

The continuous FRFT has a Hermite function with unitary variance as its eigenfunction. The corresponding eigenfunction property for the DFT would be like

$$\mathbf{F}^{2\alpha/\pi}[\hat{\mathbf{u}}_n] = e^{-jn\alpha} \hat{\mathbf{u}}_n \quad (11)$$

where $\hat{\mathbf{u}}_n$ is the eigenvector of DFT corresponding to the n th-order discrete Hermite function.

In the discussion in the previous subsection, we have known that the eigendecomposition of the DFT kernel matrix is not unique. Can the DFT have the eigenvectors with the similar shapes as the Hermite functions? These DFT eigenvectors are known as **DFT Hermite eigenvectors** in this paper.

Proposition 3: DFT Hermite eigenvectors should have the associated continuous spread variance $\sqrt{(N/2\pi)T_s}$, where T_s is the sampling intervals of signal. If the Hermite function are sampled in this way, we get

$$\phi_n(k) = \frac{1}{\sqrt{2^n n!} \sqrt{N/2}} h_n\left(\frac{k}{\sqrt{N/2\pi}}\right) e^{-(k^2\pi/N)} \quad (12)$$

where $h_n(\cdot)$ is the n th-order Hermite polynomial.

Proof: It is assumed that σ_d is the spread variance of the DFT eigenvectors. The continuous approximate form can be written as

$$\frac{1}{\sqrt{2^n n!} \sqrt{\pi} \sigma_d} h_n\left(\frac{t}{\sigma_d}\right) e^{-(t^2/2\sigma_d^2)}. \quad (13)$$

Sampling t by kT_s , (13) will become

$$\frac{1}{\sqrt{2^n n!} \sqrt{\pi} \sigma_d} h_n\left(\frac{kT_s}{\sigma_d}\right) e^{-(k^2 T_s^2 / 2\sigma_d^2)}. \quad (14)$$

The Fourier transform of (13) can be computed as

$$\frac{\sqrt{\sigma_d}}{\sqrt{2^n n!} \sqrt{\pi}} h_n(f\sigma_d) e^{-(f^2 \sigma_d^2 / 2)}. \quad (15)$$

The sampling theorem [23] tells us the continuous scope of frequency spectrum that DFT can cover is $2\pi/T_s$. Therefore, the continuous spectrum spacing (or resolution) of the DFT is equal to $2\pi/NT_s$. The variable f in (15) can be replaced by $k(2\pi/NT_s)$ to have its discrete form.

$$\frac{\sqrt{\sigma_d}}{\sqrt{2^n n! \sqrt{\pi}}} h_n\left(k \frac{2\pi}{NT_s} \sigma_d\right) e^{-(k^2 2\pi^2 \sigma_d^2 / N^2 T_s^2)}. \quad (16)$$

The variance value σ_d adjusts the scaling of Hermite function, and our goal is to adjust the variance σ_d to make the DFT of H_n have the same eigenvector shape as itself. The condition for the two shapes of (14) and (16) being the same becomes

$$\sigma_d = \sqrt{\frac{N}{2\pi}} T_s.$$

Equation (14) becomes

$$\phi_n(k) = \frac{1}{\sqrt{2^n n! \sqrt{N/2}}} h_n\left(\frac{k}{\sqrt{N/2\pi}}\right) e^{-(k^2 \pi / N)}. \quad \square$$

From Proposition 3, we can find that the DFT Hermite eigenvectors should have associate continuous spread variance $\sqrt{(N/2\pi)}T_s$. The sequence obtained from (12) is also equal to the sampling of the Hermite function with the unit variance by the sampling interval $T = \sqrt{2\pi/N}$. In Propositions 4 and 5, we will prove that even such samplings of Hermite functions can only have approximate Hermite eigenvectors of the DFT.

Proposition 4: If the sequence $\phi_n(k)$ is obtained by sampling the unit variance Hermite function with the sampling interval $T = \sqrt{2\pi/N}$, then it can be shown that

If N is even

$$(-j)^n \phi_n(k) \approx \sqrt{\frac{1}{N}} \sum_{m=-(N/2)}^{(N/2)-1} \phi_n(m) e^{-j(2\pi km/N)}. \quad (17)$$

If N is odd

$$(-j)^n \phi_n(k) \approx \sqrt{\frac{1}{N}} \sum_{m=-((N-1)/2)}^{(N-1)/2} \phi_n(m) e^{-j(2\pi km/N)} \quad (18)$$

for sufficiently large N .

Proof: Here, we only prove the case that N is even. For N odd, the proof can be easily derived in the same way. By truncating the integral interval of Fourier transform from $(-\infty, \infty)$ to $(-NT/2, NT/2)$, we have the approximation expression

$$(-j)^n \phi_n(w) \approx \frac{1}{\sqrt{2\pi}} \int_{-NT/2}^{NT/2} \phi_n(t) e^{-jw t} dt. \quad (19)$$

This approximation is valid because $NT = \sqrt{2\pi N}$ is wide for large N , and the decay rate of Gauss function $e^{-(t^2/2)}$ is very fast. Next, by replacing the continuous integral with the numerical integral, we have

$$\int_{-NT/2}^{NT/2} \phi_n(t) e^{-jw t} dt \approx \sum_{k=-(N/2)}^{(N/2)-1} \phi_n(kT) e^{-jw kT} T. \quad (20)$$

This approximation is also valid because $T = \sqrt{2\pi/N}$ is very small when N is very large. Combining (19) and (20) and letting $T = \sqrt{2\pi/N}$, we obtain

$$\begin{aligned} (-j)^n \phi_n(w) &\approx \frac{1}{\sqrt{2\pi}} \sum_{k=-(N/2)}^{(N/2)-1} \phi_n(kT) e^{-jw kT} \\ &\approx \sqrt{\frac{1}{N}} \sum_{k=-(N/2)}^{(N/2)-1} \phi_n(kT) e^{-jw kT}. \end{aligned}$$

This expression is valid for any w . Thus, taking $w = kT$ at both sides, we have

$$(-j)^n \phi_n(k) \approx \sqrt{\frac{1}{N}} \sum_{m=-(N/2)}^{(N/2)-1} \phi_n(m) e^{-j(2\pi km/N)}. \quad (21)$$

The proof is completed. \square

From the above proof, it is clear that there are two approximation errors in (17). One is the truncation error in (19), and the other is the numerical error in (20). When the value of N approaches infinity, both errors approach zero. Thus, the larger N is, the better approximation (17) is. Next, because the degree of Hermite polynomial $h_n(t)$ is n , the decay rate of the Hermite function $H_n(t)$ is proportional to $t^n e^{-t^2}$ for sufficiently large t . Thus, the larger order n is, the slower decay rate the Hermite function will have. This implies that the truncation error in (19) is larger for high-order n . Thus, when order n becomes large, the approximation in (17) becomes worse.

The n th-order continuous Hermite function should have n zeros [18]. However, these functions are not bandlimited, and the samplings in Proposition 3 cannot guarantee that the numbers of the sign changes in this sampled n th-order Hermite function are also n . The small aliasing will occur while n is closer to N , but this will not influence the development of the DFRFT. The sampled Hermite functions still can be used to construct the DFRFT kernel because they have the similar shapes and good approximations to the continuous Hermite functions.

Proposition 5: If the sequence $\bar{\phi}_n(k)$ defined in the range $[0, N-1]$ is obtained by shifting Hermite Gauss samples $\phi_n(k)$ in the following way:

If N is even

$$\bar{\phi}_n(k) = \begin{cases} \phi_n(k), & \text{for } 0 \leq k \leq \frac{N}{2} - 1 \\ \phi_n(k - N), & \text{for } \frac{N}{2} \leq k \leq N - 1 \end{cases} \quad (22)$$

and if N is odd,

$$\bar{\phi}_n(k) = \begin{cases} \phi_n(k), & \text{for } 0 \leq k \leq \frac{N-1}{2} \\ \phi_n(k - N), & \text{for } \frac{N+1}{2} \leq k \leq N - 1 \end{cases} \quad (23)$$

then it can be shown that the DFT of the $\bar{\phi}_n(k)$ can be approximated by $(-j)^n \bar{\phi}_n(k)$, i.e.,

$$(-j)^n \bar{\phi}_n(m) \approx \sqrt{\frac{1}{N}} \sum_{k=0}^{N-1} \bar{\phi}_n(k) e^{-j(2\pi km/N)} \quad (24)$$

for sufficiently large N .

Proof: Here, we also prove the case that N is even. While N is odd, the proof can also be easily derived. The DFT of the sequence $\phi_n(k)$ is given by

$$\begin{aligned} \text{DFT}(\bar{\phi}_n(k)) &= \sqrt{\frac{1}{N}} \sum_{k=0}^{N-1} \bar{\phi}_n(k) e^{-j(2\pi km/N)} \\ &= \sqrt{\frac{1}{N}} \sum_{k=0}^{(N/2)-1} \phi_n(k) e^{-j(2\pi km/N)} \\ &\quad + \sqrt{\frac{1}{N}} \sum_{k=N/2}^{N-1} \phi_n(k-N) e^{-j(2\pi km/N)}. \end{aligned} \quad (25)$$

Using the equality $e^{-j(2\pi km/N)} = e^{-j(2\pi(k-N)m/N)}$, the second term on the right side of (25) becomes

$$\begin{aligned} &\sqrt{\frac{1}{N}} \sum_{k=N/2}^{N-1} \phi_n(k-N) e^{-j(2\pi km/N)} \\ &= \sqrt{\frac{1}{N}} \sum_{l=-(N/2)}^{-1} \phi_n(l) e^{-j(2\pi ml/N)}. \end{aligned} \quad (26)$$

Substituting (26) into (25) and using Proposition 4, we obtain

$$\begin{aligned} \text{DFT}(\bar{\phi}_n(k)) &= \sqrt{\frac{1}{N}} \sum_{k=-N/2}^{(N/2)-1} \phi_n(k) e^{-j(2\pi km/N)} \quad (27) \\ &\approx (-j)^n \phi_n(m) \quad (28) \end{aligned}$$

where m is limited in the range $[0, (N/2) - 1]$. Using the equality $e^{-j(2\pi km/N)} = e^{-j(2\pi(k-N)m/N)}$, (27) can be rewritten as

$$\begin{aligned} \text{DFT}(\bar{\phi}_n(k)) &= \sqrt{\frac{1}{N}} \sum_{k=-N/2}^{(N/2)-1} \phi_n(k) e^{-j(2\pi(k-N)m/N)} \\ &\approx (-j)^n \phi_n(m-N) \end{aligned} \quad (29)$$

where m is limited in the range $[N/2, N - 1]$. Combining (28) and (29), we obtain

$$\begin{aligned} \text{DFT}(\bar{\phi}_n(k)) &= \sqrt{\frac{1}{N}} \sum_{k=0}^{N-1} \bar{\phi}_n(k) e^{-j(2\pi km/N)} \\ &\approx \begin{cases} (-j)^n \phi_n(m) & \text{for } 0 \leq m \leq \frac{N}{2} - 1 \\ (-j)^n \phi_n(m-N) & \text{for } \frac{N}{2} \leq m \leq N - 1 \end{cases} \\ &\approx (-j)^n \bar{\phi}_n(m). \end{aligned} \quad (30)$$

The proof is completed. \square

In Propositions 4 and 5, it has been proved that the samplings of Hermite functions can have approximate DFT eigenvectors. The normalized vectors for the samplings of Hermite functions are defined as

$$\mathbf{u}_n = \frac{[\bar{\phi}_n(0), \bar{\phi}_n(1), \dots, \bar{\phi}_n(N-1)]^T}{\|[\bar{\phi}_n(0), \bar{\phi}_n(1), \dots, \bar{\phi}_n(N-1)]^T\|}. \quad (31)$$

TABLE II
EIGENVALUES ASSIGNMENT RULE OF DFRFT KERNEL MATRIX

| N | the eigenvalues |
|--------|--|
| $4m$ | $e^{-jk\alpha}$, $k = 0, 1, 2, \dots, (4m-2), 4m$ |
| $4m+1$ | $e^{-jk\alpha}$, $k = 0, 1, 2, \dots, (4m-1), 4m$ |
| $4m+2$ | $e^{-jk\alpha}$, $k = 0, 1, 2, \dots, 4m, (4m+2)$ |
| $4m+3$ | $e^{-jk\alpha}$, $k = 0, 1, 2, \dots, (4m+1), (4m+2)$ |

Because matrix \mathbf{S} can have complete real orthogonal DFT eigenvectors, the eigenvectors can be used as bases for individual DFT eigensubspaces. In addition, we can compute the projections of \mathbf{u}_n in its DFT eigensubspace to obtain a Hermite-like DFT eigenvector $\tilde{\mathbf{u}}_n$

$$\tilde{\mathbf{u}}_n = \sum_{(n-k) \bmod 4=0} \langle \mathbf{u}_n, \mathbf{v}_k \rangle \mathbf{v}_k \quad (32)$$

where $k = (n \bmod 4)$, and \mathbf{v}_k is the eigenvector of matrix \mathbf{S} . $\tilde{\mathbf{u}}_n$ will be a DFT Hermite eigenvector. In (32), the DFT Hermite eigenvector $\tilde{\mathbf{u}}_n$ is computed from the eigenvectors of matrix \mathbf{S} in the same DFT eigensubspace.

C. Newly Developed DFRFT

The fractional power of matrix can be calculated from its eigendecomposition and the powers of eigenvalues. Unfortunately, there exist two types of ambiguity in deciding the fractional power of the DFT kernel matrix.

- *Ambiguity in Deciding the Fractional Powers of Eigenvalues:* We know that the square root of unity are 1 and -1 from elementary mathematics. This indicates that there exists root ambiguity in deciding the fractional power of eigenvalues.
- *Ambiguity in Deciding the Eigenvectors of the DFT Kernel Matrix:* The DFT eigenvectors constitute four major eigensubspaces; therefore, the choices for the DFT eigenvectors to construct the DFRFT kernel are multiple and not unique.

Because of the above ambiguity, we know that there are several DFRFT kernel matrices that can obey the rotation properties. The idea for developing our DFRFT is to find the discrete form for (2). In order to retain the eigenfunction property in (11), the unit variance Hermite functions are sampled with a period of $T_s = \sqrt{2\pi/N}$ in the following discussions. In the case of continuous FRFT, the terms of the Hermite functions are summed up from order zero to infinity. However, for the discrete case, only N eigenvectors for the DFT Hermite eigenvectors can be added. Table II shows the eigenvalues assignment rules for the DFRFT. This assignment rule matches the multiplicities of the eigenvalues of the DFT kernel matrix in Table I. The selections of the DFT Hermite eigenvectors are from low to high orders. It is because the approximation error of the low DFT Hermite eigenvectors are small. In addition, we should not expect that a finite vector can express the oscillation behavior of the very high-order Hermite function very well.

The transform kernel of the DFRFT can be defined as

$$\mathbf{F}^{2\alpha/\pi} = \hat{\mathbf{U}}\mathbf{D}^{2\alpha/\pi}\hat{\mathbf{U}}^T \quad (33)$$

$$= \begin{cases} \sum_{k=0}^{N-1} e^{-jk\alpha} \hat{\mathbf{u}}_k \hat{\mathbf{u}}_k^T, & \text{for } N = 4m + 1 \\ & 4m + 3 \text{ (odd)} \\ \sum_{k=0}^{N-2} e^{-jk\alpha} \hat{\mathbf{u}}_k \hat{\mathbf{u}}_k^T \\ + e^{-jN\alpha} \hat{\mathbf{u}}_N \hat{\mathbf{u}}_N^T, & \text{for } N = 4m \\ & 4m + 2 \text{ (even)} \end{cases} \quad (34)$$

where $\hat{\mathbf{U}} = [\hat{\mathbf{u}}_0|\hat{\mathbf{u}}_1|\cdots|\hat{\mathbf{u}}_{N-1}]$, whereas N is odd, and $\hat{\mathbf{U}} = [\hat{\mathbf{u}}_0|\hat{\mathbf{u}}_1|\cdots|\hat{\mathbf{u}}_{N-2}|\hat{\mathbf{u}}_N]$ for N is even. $\hat{\mathbf{u}}_k$ is the normalized eigenvector corresponding to the k th Hermite function, where \mathbf{D} is defined as follows:

For N odd

$$\mathbf{D}^{2\alpha/\pi} = \begin{bmatrix} e^{-j0} & & & & \mathbf{0} \\ & e^{-j\alpha} & & & \\ & & \ddots & & \\ & & & e^{-j\alpha(N-2)} & \\ \mathbf{0} & & & & e^{-j\alpha(N-1)} \end{bmatrix}$$

and for N even

$$\mathbf{D}^{2\alpha/\pi} = \begin{bmatrix} e^{-j0} & & & & \mathbf{0} \\ & e^{-j\alpha} & & & \\ & & \ddots & & \\ & & & e^{-j\alpha(N-2)} & \\ \mathbf{0} & & & & e^{-j\alpha N} \end{bmatrix}$$

Example 1— $N = 16$: The rotation angle α is equal to $\pi/4$, and the eigenvalues of the DFRFT are $\lambda_k = e^{-j(\pi/4)k}$ for $k = 0, 1, \dots, 14$. It must be mentioned that the last eigenvalue is not assigned to $e^{-j(\pi/4) \times 15}$ and should be assigned to the value $\lambda_{15} = e^{-j(\pi/4) \times 16}$ to match the eigenvalue multiplicities of the DFT matrix in Table I. Therefore, the transform kernel for the rotation angle α can be computed as in (34a), shown at the bottom of the page, where $\hat{\mathbf{U}} = [\hat{\mathbf{u}}_0|\hat{\mathbf{u}}_1|\cdots|\hat{\mathbf{u}}_{14}|\hat{\mathbf{u}}_{16}]$. $\hat{\mathbf{u}}_k$ is the eigenvector corresponding to the k th continuous Hermite function.

An eigenbased method for computing the DFRFT to have similar continuous results has been proposed by us in [24]–[27]. In [25], the eigenvectors obtained from matrix \mathbf{S} are directly considered to be the discrete Hermite functions. In addition, the eigenvalue–eigenfunction relation is retained in defining the DFRFT. This means that $\hat{\mathbf{u}}$ is replaced by \mathbf{v}_k in (34). Such a method is called the **S method** in this paper.

Unfortunately, the eigenvectors obtained from the matrix \mathbf{S} are just discrete Mathieu functions [21]. Although the

Mathieu functions can converge to a Hermite function [28], the convergence for the eigenvectors obtained from matrix \mathbf{S} are not so fast for the high-order Hermite functions by the LMS error criterion.

Equation (32) provides a method for finding DFT Hermite eigenvectors. The role of matrix \mathbf{S} in (32) is just as a tool to find a complete set of real and orthogonal DFT eigenvectors. However, the DFT Hermite eigenvectors obtained from (32) cannot constitute an orthogonal basis for DFT eigenspace. It is easy to verify that the angle rotation property of the DFRFT can be preserved only while the DFT eigenvectors are orthogonal. Therefore, vector orthogonalization is required for the DFT Hermite eigenvectors obtained from (32). Two methods for vector orthogonalization are proposed in the following of this paper. The DFT eigenvectors are orthogonalized for each eigensubspace. This is because the eigenvectors located in different eigensubspaces will be always orthogonal.

It is easy to show that the eigenvectors located in different eigensubspaces will be orthogonal. So the DFT Hermite eigenvectors can be orthogonalized for every eigensubspace individually to obtain orthogonal eigenvectors in the whole eigenspace of DFT. The symbol notation in developing the two algorithms are as follows:

- \mathbf{u}_n continuous Hermite samples vector;
- $\tilde{\mathbf{u}}_n$ nonorthogonalized Hermite eigenvector;
- $\hat{\mathbf{u}}_n$ orthogonalized Hermite eigenvector.

The Gram–Schmidt Algorithm (GSA): The Gram–Schmidt method [29] is a well-known orthogonalization approach for vectors. The DFT Hermite eigenvectors in each DFT eigensubspace can be orthogonalized by the Gram–Schmidt method.

Algorithm

Calculate the continuous samples of Hermite functions: \mathbf{u}_n
 Compute the eigenvectors of matrix \mathbf{S} : \mathbf{v}_n
 Using equation (32) to compute Hermite eigenvectors by projections: $\tilde{\mathbf{u}}_n$
 for $k = 0$ to 3
 $\hat{\mathbf{u}}_k = \tilde{\mathbf{u}}_k$
 for $m = 1$ to $\#(N, k) - 1$
 $p = 4m + k$
 $\hat{\mathbf{u}}_p = \tilde{\mathbf{u}}_p - \sum_{l=1}^{m-1} \langle \hat{\mathbf{u}}_p, \tilde{\mathbf{u}}_{4l+k} \rangle \hat{\mathbf{u}}_{4l+k}$
 $\hat{\mathbf{u}}_p = \frac{\hat{\mathbf{u}}_p}{\|\hat{\mathbf{u}}_p\|}$
 end
end

$$\mathfrak{R}_{\pi/4} = \mathbf{F}^{1/2}$$

$$= \hat{\mathbf{U}} \begin{bmatrix} 1 & 0 & 0 & \cdots & 0 & 0 \\ 0 & e^{-j(\pi/2) \times (1/2)} & 0 & \cdots & 0 & 0 \\ 0 & 0 & e^{-j(2\pi/2) \times (1/2)} & \cdots & 0 & 0 \\ \vdots & \vdots & \vdots & \ddots & \vdots & \vdots \\ 0 & 0 & 0 & \cdots & e^{-j(14\pi/2) \times (1/2)} & 0 \\ 0 & 0 & 0 & \cdots & 0 & e^{-j(16\pi/2) \times (1/2)} \end{bmatrix} \hat{\mathbf{U}}^T \quad (34a)$$

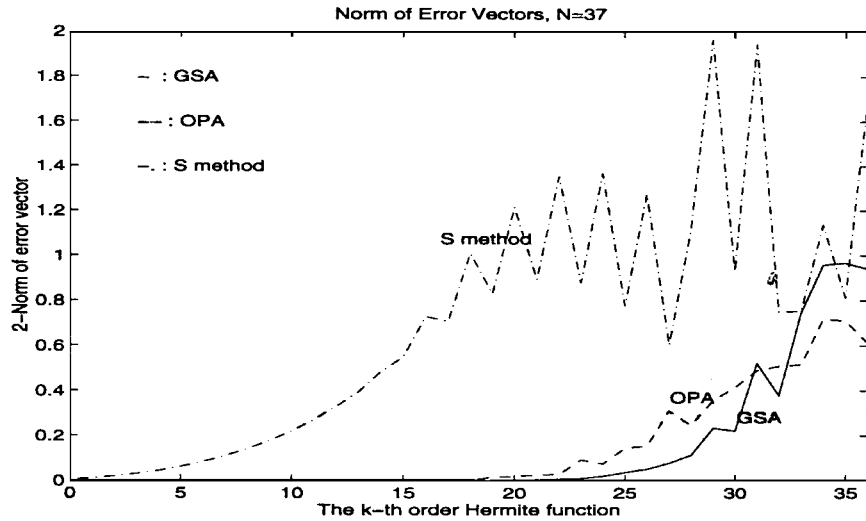


Fig. 3. Norms of error vectors between DFT Hermite eigenvectors and samples of Hermite functions.

Orthogonal Procrustes Algorithm (OPA): A traditional mathematical problem known as the *orthogonal Procrustes Algorithm* can be used to find the least Frobenius norm [30, p. 582] for the two given spaces. We can formulate our problem as the OPA to find the least Frobenius norm between the samples of Hermite functions and orthogonal DFT Hermite eigenvectors.

for $k = 0, 1, 2, 3$

$$\begin{aligned} & \text{minimize } \|\mathbf{U}_k - \hat{\mathbf{U}}_k\|_F \\ & = \text{minimize } \|\mathbf{U}_k - \mathbf{Q}_k \mathbf{V}_k\|_F \quad \text{subject to } \mathbf{Q}_k^T \mathbf{Q}_k = \mathbf{I} \end{aligned} \quad (35)$$

$$(36)$$

where $\|\cdot\|_F$ is the Frobenius norm of the matrix, $\mathbf{V}_k = [\mathbf{v}_k | \mathbf{v}_{k+4} | \cdots | \mathbf{v}_{k+(z(N,k)-1)*4}]$, $\mathbf{U}_k = [\mathbf{u}_k | \mathbf{u}_{k+4} | \cdots | \mathbf{u}_{k+(z(N,k)-1)*4}]$, and $\hat{\mathbf{U}}_k = [\hat{\mathbf{u}}_k | \hat{\mathbf{u}}_{k+4} | \cdots | \hat{\mathbf{u}}_{k+(z(N,k)-1)*4}] = \mathbf{Q}_k \mathbf{V}_k$ will be our solution. The minimizing \mathbf{Q}_k can be found by calculating the singular value decomposition (SVD) of $\mathbf{V}_k^T \mathbf{U}_k$. Because the $\mathbf{V}_k^T \mathbf{V}_k = \mathbf{I}$, the solution $\hat{\mathbf{U}}_k$ will also satisfy $\hat{\mathbf{U}}_k^T \hat{\mathbf{U}}_k = \mathbf{I}$.

Algorithm

Calculate the continuous samples of Hermite functions: \mathbf{u}_n
 Compute the eigenvectors of \mathbf{S} : \mathbf{v}_n
 Using equation (32) to compute Hermite eigenvectors by projections: $\tilde{\mathbf{u}}_n$
 for $k = 0$ to 3
 $\mathbf{C}_k = \mathbf{V}_k^T \mathbf{U}_k$
 Compute the SVD of \mathbf{C}_k , $\mathbf{C}_k = \mathbf{A}_k \mathbf{D}_k \mathbf{B}_k^T$
 $\mathbf{Q}_k = \mathbf{A}_k \mathbf{B}_k^T$
 $\hat{\mathbf{U}}_k = \mathbf{Q}_k \mathbf{V}_k$
 end

The GSA minimizes the errors between the samples of Hermite functions and orthogonal DFT Hermite eigenvectors from low to high orders, and the OPA minimizes the total errors between the samples of Hermite functions and orthogonal DFT Hermite eigenvectors. In Fig. 3, the norms of error vectors between the computed DFT Hermite eigenvectors and

samples of Hermite functions are plotted for $N = 37$. The error vectors between samples of Hermite functions and DFT Hermite eigenvectors are defined as

$$\mathbf{e}_n = \mathbf{u}_n - \hat{\mathbf{u}}_n. \quad (37)$$

Example 2: In this example, we use the DFRFT to deal with the rectangular window function shown in Fig. 1. The sampling interval T_s is equal to $4/13$, and the number of points N is equal to 73. The sampled discrete data then becomes $[N = 73, x(n) = 1, -6 \leq n \leq 6; \text{ otherwise, } x(n) = 0]$, which is the same as the signal used in Fig. 2. Figs. 4–6 show the DFRFT of the rectangular window function for various angles for S method, GSA, and OPA, respectively.

Example 3: The DFRFT by the GSA for a chirp signal is computed in this example. The chirp signal used here is equal to $e^{j \times 0.1141k^2}$, where $k = -32, \dots, 32$. In Fig. 7, it can be found that the transform results change from a chirp signal ($\alpha = 0$) to an impulse-like function ($\alpha = 3\pi/7$). Therefore, the DFRFT can be used for the chirp signal and chirp rate detection. A more detailed theory and algorithm can be found in [7].

D. Properties of DFRFT

The properties of the DFRFT are shown in Table III. Transform results of the impulse signal ($N = 37$) are plotted in Figs. 8–10 for the S method, GSA, and OPA, respectively. The corresponding samples of the continuous FRFT for the impulse signal are plotted in Fig. 11. The norm of the error vectors between the DFRFT and samples of the FRFT are also shown in the titles of Figs. 8–10.

The continuous FRFT is an orthonormal signal decomposition for chirp signals [9]. Based on the unitary property in the DFRFT and the transform results shown in Figs. 9 and 10, we can find that the proposed DFRFT provides a similar orthonormal signal decomposition for discrete chirp-like signals.

E. Implementation of the New DFRFT

As in the case of DFT frequency domain, the last half of the indices in the DFRFT must also be treated as the negative

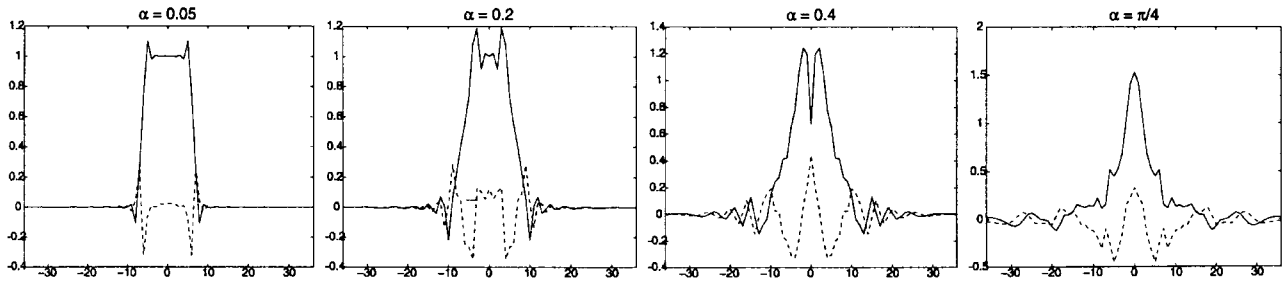


Fig. 4. DFRFT by S method of a rectangular window function. $x(n) = 1$ when $-6 \leq n \leq 6$, and $x(n) = 0$ otherwise. The output is close to the continuous FRFT in Fig. 1.

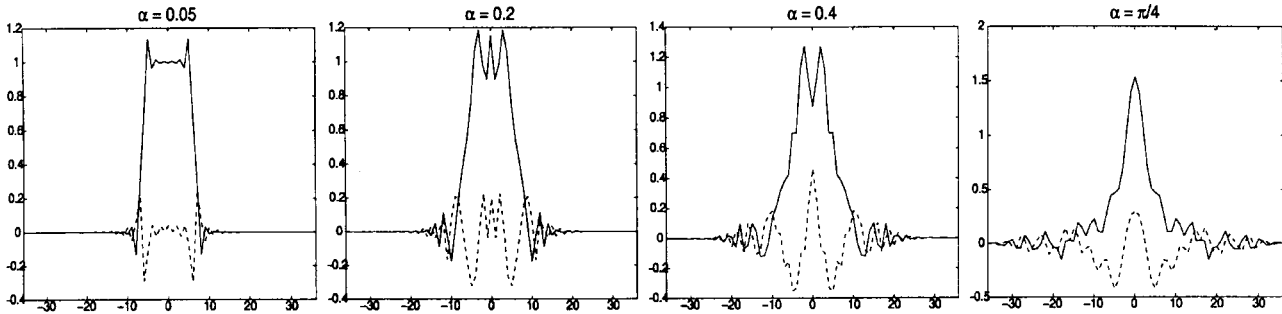


Fig. 5. DFRFT by GSA method of a rectangular window function. $x(n) = 1$ when $-6 \leq n \leq 6$, and $x(n) = 0$ otherwise. This figure has a closer output to the continuous FRFT than Fig. 4.

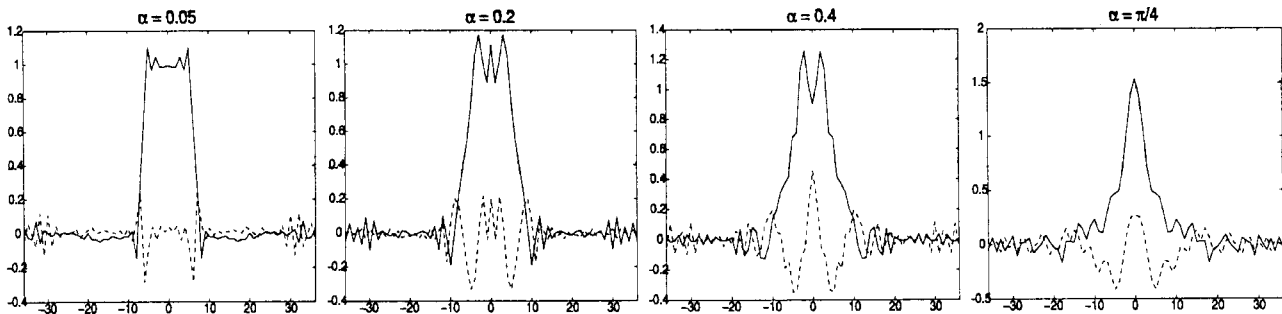


Fig. 6. DFRFT by OPA method of a rectangular window function. $x(n) = 1$ when $-6 \leq n \leq 6$, and $x(n) = 0$ otherwise. This figure has a closer output to the continuous FRFT than Fig. 4.

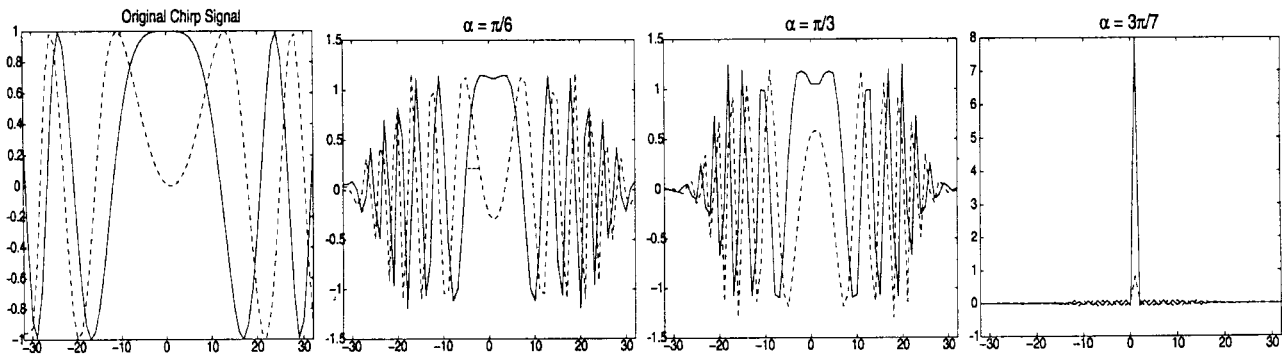


Fig. 7. DFRFT by GSA of a chirp signal. $e^{j \times 0.1141k^2}$, $k = -32 \dots 32$. When $\alpha = 3\pi/7$, an impulse-like output is obtained.

frequency. This concept is also applied in the time domain ($\alpha = 0$, identity transform) and any angle transform domains.

When the number of points N and the rotation angle α are determined, the DFT Hermite eigenvectors can be computed *a priori*, and the eigenvalues of DFRFT are also determined. Then, the computation of the DFRFT can be implemented only by a transform kernel matrix multiplication. The complexity of

computing the DFRFT is $\mathcal{O}(N^2)$, and it is the same as in the DFT case. If the rotational angles are adjusting, the following method for implementing the DFRFT can be applied:

$$\mathbf{A} = \hat{\mathbf{U}}^T \mathbf{x} \tag{38}$$

$$\begin{aligned} \mathbf{F}^{2\alpha/\pi} &= \hat{\mathbf{U}} \mathbf{D}^{2\alpha/\pi} \hat{\mathbf{U}}^T \mathbf{x} \\ &= \hat{\mathbf{U}} \cdot \mathbf{D}^{2\alpha/\pi} \cdot \mathbf{A} \end{aligned} \tag{39}$$

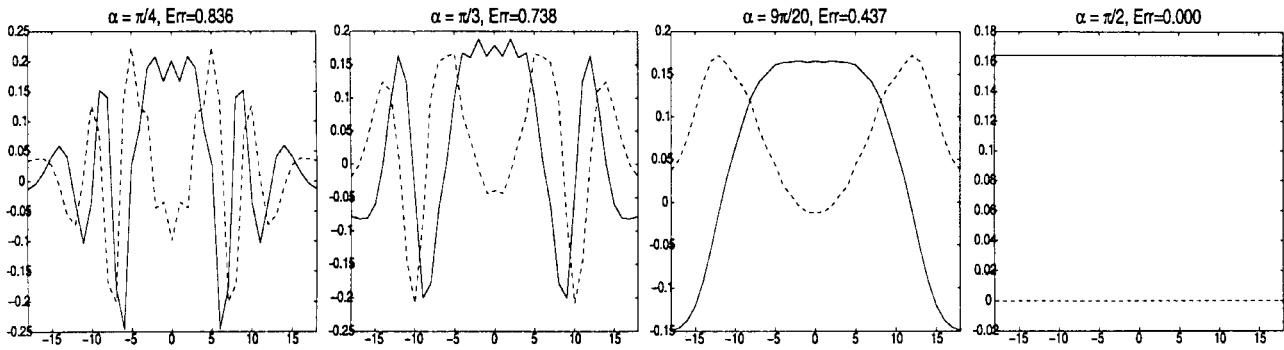


Fig. 8. DFRFT by S method of an impulse function. $x(0) = 1$, and $x(n) = 0$ otherwise. It can be seen that chirp-like outputs are obtained while the angle $\alpha \neq \pi/2$. When $\alpha = \pi/2$, the DFRFT reduces to DFT, and the output becomes a constant.

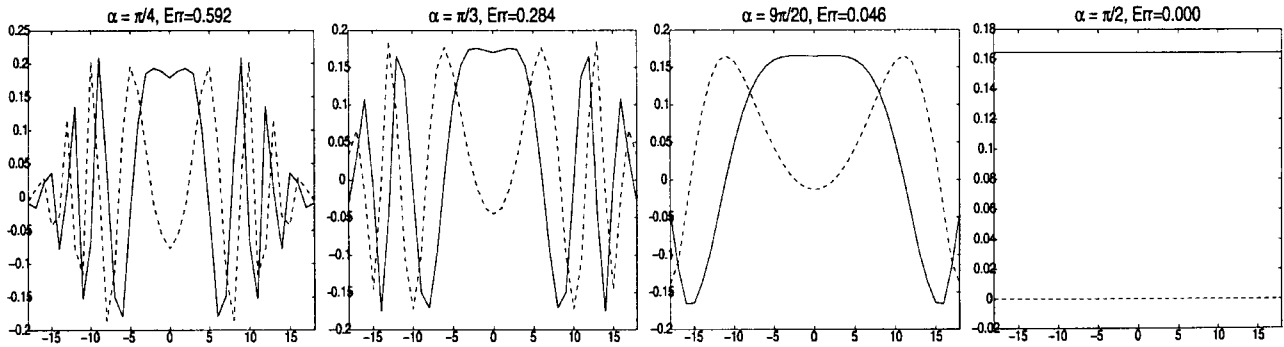


Fig. 9. DFRFT by GSA of an impulse function. $x(0) = 1$, and $x(n) = 0$ otherwise. It can be seen that chirp-like outputs are obtained while the angle $\alpha \neq \pi/2$. When $\alpha = \pi/2$, the DFRFT reduces to DFT, and the output becomes a constant.

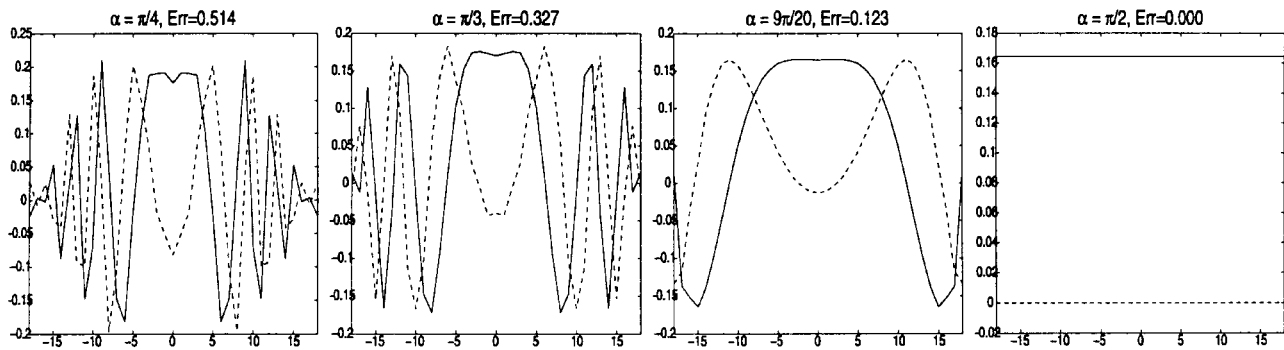


Fig. 10. DFRFT by OPA of an impulse function. $x(0) = 1$, and $x(n) = 0$ otherwise. It can be seen that chirp-like outputs are obtained while the angle $\alpha \neq \pi/2$. When $\alpha = \pi/2$, the DFRFT reduces to DFT, and the output becomes a constant.

$$= \sum_{k=0}^{N-1} a_k e^{-jk\alpha} \hat{\mathbf{u}}_k. \quad (40)$$

The definitions of matrix $\hat{\mathbf{U}}$ and matrix \mathbf{D} are the same as those in (33). $\mathbf{A} = [a_0, a_1, \dots, a_{N-1}]^T$. The coefficients a_k 's are the inner products of signal and eigenvectors, and they can be computed in advance. If the rotation angle is changed, only the diagonal matrix $\mathbf{D}^{2\alpha/\pi}$ should be recomputed.

F. Discussion

The method in [17] obeys the rotation properties, but it cannot have similar results as in the continuous case. A rigorous discussion for the mismatches of [17] has been presented in [16]. Here, we stress the major reason for this mismatch.

Proposition 6: The method in (6) assigns all the eigenvectors of the DFRFT matrix to only four different eigenvalues. This is the major reason for the mismatches in [17].

Proof: Let \mathbf{v} be any DFT eigenvector located in the eigensubspace E_k . $\mathbf{F}\mathbf{v} = e^{-j(\pi/2)k}\mathbf{v}$. Applying the transform kernel defined in (6) to the eigenvector \mathbf{v} , we can obtain

$$\begin{aligned} \mathbf{F}^t \mathbf{v} &= a_0(t)\mathbf{v} + a_1(t)\mathbf{F}\mathbf{v} + a_2(t)\mathbf{F}^2\mathbf{v} + a_3\mathbf{F}^3(t)\mathbf{v} \\ &= a_0(t)\mathbf{v} + a_1(t)e^{-j(\pi/2)k}\mathbf{v} + a_2(t)e^{-j\pi k}\mathbf{v} \\ &\quad + a_3(t)e^{-j(3\pi/2)k}\mathbf{v} \\ &= \left[a_0(t) + e^{-j(\pi/2)k}a_1(t) + e^{-j\pi k}a_2(t) \right. \\ &\quad \left. + e^{-j(3\pi/2)k}a_3(t) \right] \mathbf{v}. \end{aligned}$$

Therefore, \mathbf{v} is also a DFRFT eigenvector, and the value $a_0(t) + e^{-j(\pi/2)k}a_1(t) + e^{-j\pi k}a_2(t) + e^{-j(3\pi/2)k}a_3(t)$ is the eigenvalue for this eigenvector \mathbf{v} . Since any eigenvector in

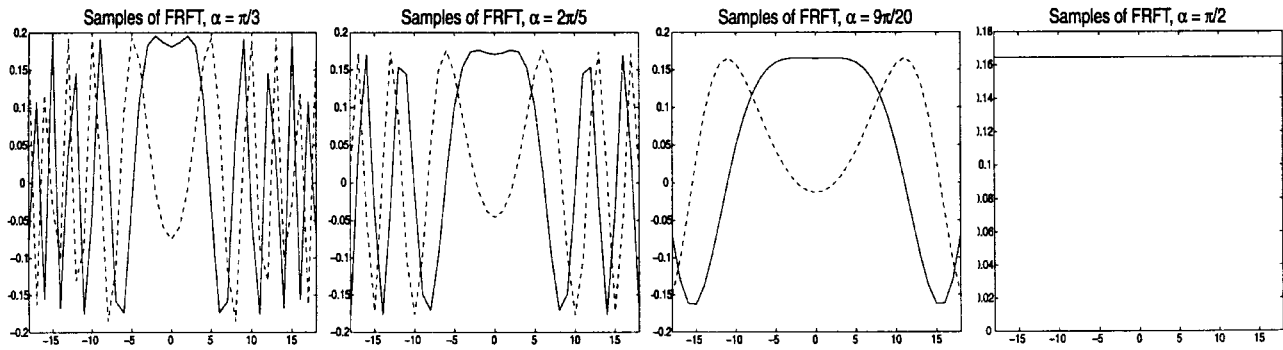


Fig. 11. Samples of continuous FRFT of an impulse function. $x(0) = 1$, and $x(t) = 0$ otherwise.

TABLE III
PROPERTIES OF DFRFT

| | |
|-------------------|---|
| Unitary | $(\mathbf{F}^{\frac{2\alpha}{\pi}})^* = (\mathbf{F}^{\frac{2\alpha}{\pi}})^{-1} = \mathbf{F}^{-\frac{2\alpha}{\pi}}$ |
| Angle additivity | $\mathbf{F}^{\frac{2\alpha}{\pi}} \mathbf{F}^{\frac{2\beta}{\pi}} = \mathbf{F}^{\frac{2(\alpha+\beta)}{\pi}}$ |
| Time Inversion | $\mathbf{F}^{\frac{2\alpha}{\pi}} x(-n) = \mathbf{X}_\alpha(-n)$ |
| Periodicity | $\mathbf{F}^{\frac{\alpha+2\pi}{\pi}} = \mathbf{F}^{\frac{2\alpha}{\pi}}$ |
| Symmetry | $\mathbf{F}^{\frac{2\alpha}{\pi}}(a, b) = \mathbf{F}^{\frac{2\alpha}{\pi}}(b, a)$ where $\mathbf{F}^{\frac{2\alpha}{\pi}}(a, b)$ is the (a, b) -element in DFRFT kernel matrix |
| Eigenfunction | $\mathbf{F}^{\frac{2\alpha}{\pi}}[\mathbf{v}_n] = e^{-j\alpha n} \mathbf{v}_n$ where \mathbf{v}_n is Hermite-like function |
| Impulse Transform | $\mathbf{F}^{\frac{2\alpha}{\pi}}[\delta(k)] \approx \sqrt{\frac{N}{2\pi}} \sqrt{\frac{1-j \cot \alpha}{2\pi}} e^{j\frac{\alpha}{2} \cot \alpha}$ |
| Parity | If \mathbf{x} is even, \mathbf{X}_α is even. If \mathbf{x} is odd, \mathbf{X}_α is odd. |

one of the four eigensubspace E_k has the same eigenvalue, the method assigns the DFRFT eigenvalues to only four values. \square

In the DFRFT of [17], there will be four different eigenvalues for all the eigenvectors. On the other hand, the proposed DFRFT has assigned a different eigenvalue for each eigenvector. The development of the new DFRFT is based on the same idea as (2), which satisfies the eigenvalue and eigenfunction relationship as a continuous FRFT kernel.

$$\mathbf{F}^{2\alpha/\pi}[\hat{\mathbf{u}}_n] = e^{-jn\alpha} \hat{\mathbf{u}}_n \quad (41)$$

where $\hat{\mathbf{u}}_n$ is the eigenvector corresponding to the n th-order Hermite function. It should be noted that the number of eigenfunctions for the continuous FRFT in (2) is infinite. However, the number of DFT Hermite eigenvectors is only finite, and there are some approximation errors in the DFT Hermite eigenvectors. While N approaches infinity, the approximation errors of the DFT Hermite eigenvectors will be reduced, and more DFT Hermite eigenvectors are used to compute the DFRFT.

In [31], an alternative DFRFT has recently been proposed. It is based on retaining the property of the DFT that a sampled periodic function transforms into a periodic function. Thus, the signal and transform results in [31] are discrete and periodic, and the rotation angle α in [31] is valid for a certain discrete set of rotation angles. Moreover, the periods in the transform results change for different rotation angles. The DFRFT developed in this paper is based on the mimicking of the eigenvalue–eigenfunction relationship that the continuous

counterpart of this transform has with the normalized unit variance Hermite functions. Therefore, our DFRFT can be used for any rotation angle and can provide very similar results as continuous cases.

IV. RELATIONSHIP BETWEEN FRFT AND DFRFT

In this section, we will establish the relationship between the FRFT and the DFRFT. Then, the DFRFT can be used to give the similar continuous transform results within the accuracy of the discrete finite vector approximation.

A. Transform Range and Resolution of DFRFT

In this subsection, we will discuss the transform range and resolution for the DFRFT (see Table IV). In the conventional DFT analysis, the transform range and resolution of the DFT have been well discussed [23]. To begin with, we will review and understand the transform range and resolution for the conventional DFT. In the following discussion, T_s is the sampling interval for the original continuous signal; it is also the time resolution, N is the number of points of the discrete signal, and NT_s is the total recorded signal duration and is the $\alpha = 0$ transform range in the time domain as well. The overall frequency range that the DFT can represent is equal to $T_s/2\pi$, and the frequency resolution is $2\pi/NT_s$ [23].

In Proposition 3, it has been proved that the spread variance of the DFT Hermite eigenvector is $\sqrt{(N/2\pi)}T_s$. Here, we will compute the FRFT for a Hermite function with any variance σ .

TABLE IV
TRANSFORM RANGE AND RESOLUTION OF DFRFT

| | Time domain ($\alpha = 0$) | Fractional Fourier domain ($0 < \alpha < \frac{\pi}{2}$) | Frequency domain ($\alpha = \frac{\pi}{2}$) |
|-----------------|---------------------------------|---|--|
| Transform Range | $N \Delta t = NT_s$ | $N \Delta_\alpha = \sqrt{N^2 T_s^2 \cos^2 \alpha + \frac{4\pi^2}{T_s^2} \sin^2 \alpha}$ | $N \Delta f = \frac{2\pi}{T_s}$ |
| Resolution | $\Delta t = T_s$ | $\Delta_\alpha = \sqrt{T_s^2 \cos^2 \alpha + \frac{4\pi^2}{N^2 T_s^2} \sin^2 \alpha}$ | $\Delta f = \frac{2\pi}{NT_s}$ |

Proposition 7: The continuous FRFT of a Hermite function with variance σ is equal to

$$\begin{aligned} \mathcal{F}^{2\alpha/\pi}[H_{\sigma,n}] &= \sqrt{\sigma_\alpha} \sqrt{\frac{1 - j \cot \alpha}{1 - j \sigma^2 \cot \alpha}} \\ &\cdot \exp\left(j \frac{u^2}{2} \cot \alpha \left(1 - \frac{\cos^2 \beta}{\cos^2 \alpha}\right)\right) \\ &\cdot e^{-jn\beta} H_{\sigma_\alpha, n}(u) \end{aligned} \quad (42)$$

where $\beta = \tan^{-1}(\tan \alpha / \sigma^2)$. The new variance σ_α is computed as

$$\sigma_\alpha = \sqrt{\sigma^2 \cos^2 \alpha + \frac{\sin^2 \alpha}{\sigma^2}}. \quad (43)$$

Proof: This proposition can be easily proved by computing the FRFT of the normalized Hermite functions. \square

It is easy to check some special cases for (43): $\sigma_0 = \sigma$ and $\sigma_{\pi/2} = 1/\sigma$. If $\sigma = 1$, σ_α will be equal to 1 for any value of α . In (42), only the last term $H_{\sigma_\alpha, n}$ can affect the envelope of the FRFT of $H_{\sigma, n}$.

From Propositions 4 and 5, it has been shown that there are approximation errors in the DFT Hermite eigenvectors. For simplification of analysis, the approximation errors of the DFT Hermite eigenvectors are ignored in the following discussion. The symbol Δ_α is used to denote the resolution of the FRFT. $\Delta_0 = T_s$ and $\Delta_{\pi/2} = 2\pi/T_s$ are the two special cases.

Proposition 8: The resolution of the DFRFT with angular parameter α is equal to

$$\Delta_\alpha = \sqrt{T_s^2 \cos^2 \alpha + \frac{4\pi^2}{N^2 T_s^2} \sin^2 \alpha} \quad (44)$$

where T_s is the sampling interval of the signal, and N is the number of points for the discrete signal. The overall transform range of the DFRFT can cover is equal to

$$N \Delta_\alpha = \sqrt{N^2 T_s^2 \cos^2 \alpha + \frac{4\pi^2}{T_s^2} \sin^2 \alpha}. \quad (45)$$

Proof: From Proposition 3, it has been known that the spread variance of the DFRFT is $\sqrt{(N/2\pi)T_s}$. The sampled vector in (12) can also be an approximate eigenvector in the fractional Fourier domain (angle α).

$$\frac{1}{\sqrt{2^n n!} \sqrt{N/2}} h_n \left(\frac{k \Delta_\alpha}{\sqrt{N/2\pi}} \right) e^{-(k^2 \Delta_\alpha^2 \pi / N)}. \quad (46)$$

Thus, the spread variance of the DFRFT for angle α is equal to

$$\sqrt{\frac{N}{2\pi}} \Delta_\alpha. \quad (47)$$

Moreover, we can substitute the variance in (43) by $\sqrt{(N/2\pi)T_s}$ to get the spread variance of the DFRFT in the fractional Fourier domain (angle α)

$$\sqrt{\frac{N}{2\pi} T_s^2 \cos^2 \alpha + \frac{2\pi}{N T_s^2} \sin^2 \alpha}. \quad (48)$$

Both (47) and (48) indicate the corresponding variance of DFT Hermite eigenvectors in the fractional Fourier domain; therefore, the resolution of the FRFT can be obtained as

$$\Delta_\alpha = \sqrt{T_s^2 \cos^2 \alpha + \frac{4\pi^2}{N^2 T_s^2} \sin^2 \alpha}. \quad (49)$$

The overall transform range the DFRFT can cover is equal to

$$N \Delta_\alpha = \sqrt{N^2 T_s^2 \cos^2 \alpha + \frac{4\pi^2}{T_s^2} \sin^2 \alpha}. \quad (50)$$

\square

In (34), the DFRFT performs independent circular rotation in the discrete notation. From (45) and Fig. 12, it can be found that the signal rotation of the DFRFT is an elliptical rotation in the continuous time–frequency plane, whereas $T_s \neq \sqrt{2\pi/N}$. This means that the DFRFT is implemented in a circular rotation for the discrete case, but it actually performs elliptical rotation in the continuous time–frequency plane. Three cases can be realized for the signal rotation of the DFRFT in the continuous time–frequency plane.

- The lengths of time and frequency ranges are equal ($T_s = \sqrt{2\pi/N}$).
- The length of the time range is longer than that of the frequency ($T_s > \sqrt{2\pi/N}$).
- The length of the time range is shorter than that of the frequency ($T_s < \sqrt{2\pi/N}$).

The rotation concept of the DFRFT in the continuous time–frequency plane is plotted in Fig. 12. Angle β is the actual angle for the elliptical rotation, as drawn in Fig. 12.

B. Elliptical Rotation versus Circular Rotation

The FRFT performs circular rotation in the continuous time–frequency plane, but the DFRFT performs elliptical rotation in the continuous time–frequency plane while $T_s \neq \sqrt{2\pi/N}$. In this subsection, we will define circular and elliptical rotations clearly and establish the relationship between circular and elliptical rotations.

- *Circular Rotation:*

$$\mathfrak{R}_\alpha(t, u) = \sum_n e^{-jn\alpha} H_n(t) H_n(u) \quad (51)$$

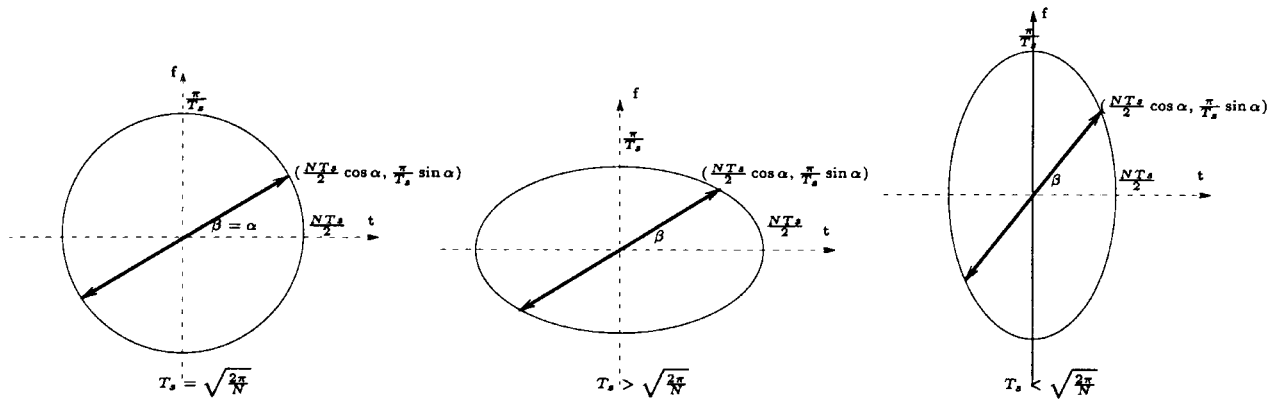


Fig. 12. Three different cases of rotation concept for DFRFT in continuous time-frequency plane.

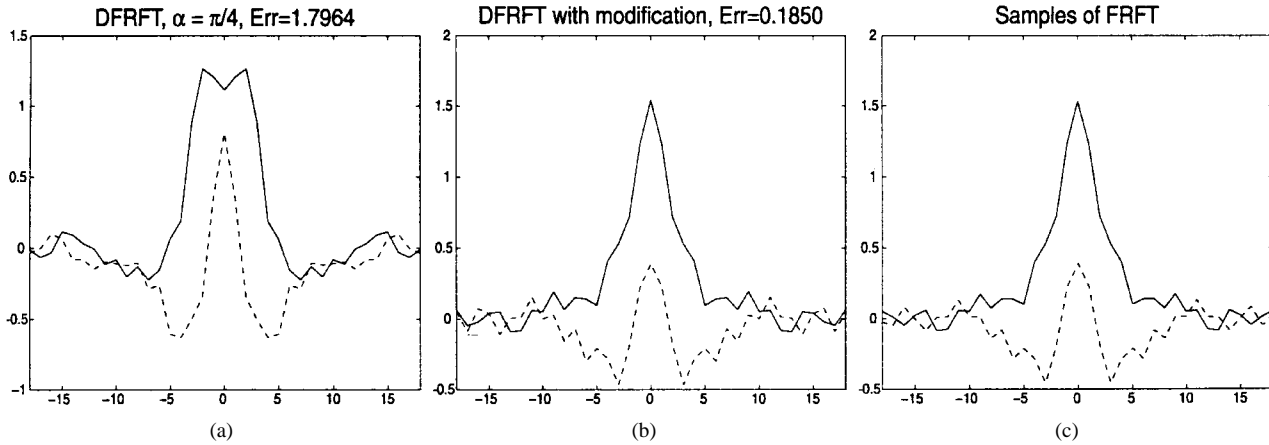


Fig. 13. Results of Example 4 showing that the error norms between DFRFT and continuous FRFT samples are greatly reduced by angle modification and post-phase compensation.

$$\mathcal{X}_\alpha(u) = \int_t \mathfrak{R}_\alpha(t, u)x(t) dt \quad (52)$$

$$= \sum_n e^{-jn\alpha} H_n(u) \int H_n(t)x(t) dt \quad (53)$$

where \mathfrak{R}_α is the transform kernel of circular rotation. $\mathcal{X}_\alpha(u)$ is the circular rotation of signal $x(t)$.

• *Elliptical Rotation:*

$$\hat{\mathfrak{R}}_\alpha(t, u) = \sum_n e^{-jn\alpha} H_{\sigma, n}(t) H_{\sigma, n}(u) \quad (54)$$

$$\hat{\mathcal{X}}_\alpha(u) = \int_t \hat{\mathfrak{R}}_\alpha(t, u)x(t) dt \quad (55)$$

$$= \sum_n e^{-jn\alpha} H_{\sigma, n}(u) \int H_{\sigma, n}(t)x(t) dt \quad (56)$$

where $\hat{\mathfrak{R}}_\alpha$ is the transform kernel of elliptical rotation, and σ_α is defined as in (43). $\hat{\mathcal{X}}_\alpha(u)$ is the elliptical rotation of signal $x(t)$. While $\sigma = 1$, the elliptical rotation will become the circular rotation.

The transform kernels of the circular and elliptical rotations defined above are infinite numbers of sums for Hermite eigenvectors. The critical point for which we care is the

spread variance changes in these two schemes. If the Hermite eigenvectors in the circular rotation are from order 0 to infinity, the circular rotation is just the FRFT of the signal.

Proposition 9: The circular rotation of signal $x(t)$ can be implemented by an angle modification of the elliptical rotation and post-multiplying a phase compensation factor.

$$\mathcal{X}_\alpha(u) = P_C \hat{\mathcal{X}}_\beta\left(u \frac{\sigma_\beta}{\sigma_\alpha}\right) \quad (57)$$

where $\beta = \tan^{-1}(\tan \alpha / \sigma^2)$, and the post-phase compensation factor is equal to

$$P_C = \sqrt{\sigma_\beta} \sqrt{\frac{1 - j \cot \alpha}{1 - j \sigma^2 \cot \alpha}} \cdot \exp\left(j \frac{u^2}{2} \cot \alpha \left(1 - \frac{\cos^2 \beta}{\cos^2 \alpha}\right)\right). \quad (58)$$

Proof: The signal $x(t)$ can be written as the weighted sum of the normalized Hermite functions.

$$x(t) = \sum_n D_n H_{\sigma, n}(t) \quad (59)$$

where $D_n = \int_t x(t)H_{\sigma,n}(t)dt$. Compute the FRFT of $x(t)$ (circular rotation) for the both sides of (59).

$$\begin{aligned}
\mathcal{X}_\alpha(u) &= \sum_n D_n \mathfrak{R}_\alpha[H_{\sigma,n}(t)] \\
&= \sum_n D_n \sqrt{\sigma_\alpha} \sqrt{\frac{1-j \cot \alpha}{1-j\sigma^2 \cot \alpha}} \\
&\quad \cdot \exp\left(j \frac{u^2}{2} \cot \alpha \left(1 - \frac{\cos^2 \beta}{\cos^2 \alpha}\right)\right) \\
&\quad \cdot e^{-jn\beta} H_{\sigma_\alpha,n}(u) \\
&= \sqrt{\sigma_\alpha} \sqrt{\frac{1-j \cot \alpha}{1-j\sigma^2 \cot \alpha}} \\
&\quad \cdot \exp\left(j \frac{u^2}{2} \cot \alpha \left(1 - \frac{\cos^2 \beta}{\cos^2 \alpha}\right)\right) \\
&\quad \cdot \sum_n e^{-jn\beta} H_{\sigma_\alpha,n}(u) \cdot D_n \\
&= \sqrt{\sigma_\alpha} \sqrt{\frac{1-j \cot \alpha}{1-j\sigma^2 \cot \alpha}} \\
&\quad \cdot \exp\left(j \frac{u^2}{2} \cot \alpha \left(1 - \frac{\cos^2 \beta}{\cos^2 \alpha}\right)\right) \\
&\quad \cdot \sqrt{\frac{\sigma_\beta}{\sigma_\alpha}} \sum_n e^{-jn\beta} H_{\sigma_\beta,n}\left(u \frac{\sigma_\beta}{\sigma_\alpha}\right) \\
&\quad \cdot \int_t x(t)H_{\sigma,n}(t) dt \\
&= \sqrt{\sigma_\beta} \sqrt{\frac{1-j \cot \alpha}{1-j\sigma^2 \cot \alpha}} \\
&\quad \cdot \exp\left(j \frac{u^2}{2} \cot \alpha \left(1 - \frac{\cos^2 \beta}{\cos^2 \alpha}\right)\right) \hat{\mathcal{X}}_\beta\left(u \frac{\sigma_\beta}{\sigma_\alpha}\right).
\end{aligned}$$

The operation in the DFRFT performs elliptical rotation in the continuous time–frequency plane for the case $T_s \neq \sqrt{2\pi/N}$. Using Proposition 9, the elliptical rotation can be implemented by circular rotation. If the values of (57) are evaluated at the points $k\Delta_\alpha$, it will become

$$\mathcal{X}_\alpha(k\Delta_\alpha) = P_D \hat{\mathcal{X}}_\beta\left(k\Delta_\alpha \frac{\sigma_\beta}{\sigma_\alpha}\right) \quad (60)$$

$$= P_D \hat{\mathcal{X}}_\beta(k\Delta_\beta). \quad (61)$$

Equation (61) indicates that the FRFT with angle α can be implemented by a DFRFT with angle β , and the transform resolution is still Δ_α . The discrete post-phase compensation factor for the DFRFT is

$$\begin{aligned}
P_D &= \sqrt{\frac{\sigma^2 - j\sigma^2 \cot \alpha}{1 - j\sigma^2 \cot \alpha}} \\
&\quad \cdot \exp\left(j \frac{k^2 \Delta_\alpha^2}{2} \cot \alpha \left(1 - \frac{\cos^2 \beta}{\cos^2 \alpha}\right)\right) \quad (62)
\end{aligned}$$

where $\sigma = \sqrt{(N/2\pi)T_s}$. It must be noted that the postphase compensation factors in (58) and (62) are different. The variable σ_β in (58) is replaced by σ in (62) for preserving the unitary property in the DFRFT. If $T_s \approx \sqrt{2\pi/N}$, the variance of the continuous-time counterpart of the eigenvector will approximate to unity, and the effects of angle modification and postphase compensation will be very small. In this case,

the length of time range (NT_s) will almost equal the length of the frequency range ($2\pi/T_s$). The rotation will almost be a circular rotation. While the variance is far from unity, the following steps must be used to make the results of discrete cases match those of the continuous case.

Step 1) Compute the modification angle $\beta = \tan^{-1}((2\pi/NT_s^2) \tan \alpha)$.

Step 2) Calculate the N -point DFRFT of the signal with the angular parameter β .

Step 3) Multiply the result obtained from Step 2 by the post-phase compensation factor shown in (62).

In Example 2, we directly compute the DFRFT without angle modification and postphase compensation. The corresponding variance $\sqrt{(N/2\pi)T_s}$ is equal to 1.0488 in Example 2. The length of the time range is almost equal to the length of the frequency range; therefore, the DFRFT in Example 2 is almost a circular rotation.

Example 4: In this example, we again deal with the rectangular window shown in Example 2. However, the sampling interval is still $T_s = 4/13$, and the number of points in the signal becomes 37. Here, we only compute the results of rotation angle α , which are equal to $\pi/4$ by the GSA. The continuous counterpart of the variance σ in this example is $\sqrt{(N/2\pi)T_s} \approx 0.7467$. Therefore, the modification of the angle and postphase compensation discussed above are very critical. Fig. 13(a) shows the DFRFT with angular parameter $\pi/4$ for the original signal. Fig. 13(b) is the DFRFT with angular parameter modification and postphase compensation. Fig. 13(c) shows the sample values of the continuous FRFT for the indices $k\Delta_\alpha$, where $k = -18, -17, \dots, 18$, $\Delta_\alpha = \sqrt{(T_s^2/2) + (\pi/NT_s^2)}$. The results shown in Fig. 13(b) match the corresponding continuous FRFT cases shown in Fig. 13(c) very well, and Fig. 13(a) is quite different from Fig. 13(c) due to the elliptical rotation and not in the circular rotation in the continuous time–frequency plane.

V. CONCLUSIONS

The development of this DFRFT is based on the eigendecomposition of the DFT kernel matrix \mathbf{F} . The new transform retains the eigenvalue–eigenfunction relationship using the sampled version of the normalized unit-variance Hermite functions that the continuous FRFT has with the unit variance Hermite functions. With the help of the commutative matrix \mathbf{S} , the complete real and orthonormal eigenvectors of the DFT kernel matrix can be computed. The DFT Hermite eigenvectors can be calculated by the projection of samples of the unit variance Hermite functions in the DFT eigensubspaces through the help of the eigenvectors of the matrix \mathbf{S} . However, such DFT Hermite eigenvectors cannot form an orthogonal basis for the DFT eigenspaces. Two vector orthogonalization processes for the DFT Hermite eigenvectors are accordingly proposed in this paper: One is GSA, and the other is OPA. The GSA minimizes the errors between the samples of the Hermite functions and the orthogonal DFT Hermite eigenvectors from low to high orders, whereas the OPA minimizes the total errors between the samples of the Hermite functions and the orthogonal DFT Hermite eigenvectors.

Furthermore, the relationship between the FRFT and the DFRFT can be established as follows. If $T_s = \sqrt{2\pi/N}$, the DFRFT performs a circular rotation of the signal in the time–frequency plane. On the other hand, if $T_s \neq \sqrt{2\pi/N}$, the DFRFT becomes an elliptical rotation in the continuous time–frequency plane. An angle modification and a postphase compensation in the DFRFT for elliptical rotation are required to match the results that are similar for the continuous FRFT.

The DFRFT proposed in this paper not only supplies the similar transforms to match with those of the continuous case but also preserves the rotation properties. The complexity for implementing the DFRFT is $\mathcal{O}(N^2)$, which is the same as that of the DFT. This DFRFT provides a method for implementing the discrete FRFT, and it is an important tool for signal processing.

REFERENCES

- [1] R. N. Bracewell, *The Fourier Transform and Its Applications*, 2nd ed. New York: McGraw-Hill, 1986.
- [2] A. C. McBride and F. H. Kerr, "On Namias' fractional Fourier transforms," *IMA J. Appl. Math.*, vol. 39, pp. 159–175, 1987.
- [3] V. Namias, "The fractional order Fourier transform and its application to quantum mechanics," *J. Inst. Math. Applicat.*, vol. 25, pp. 241–265, 1980.
- [4] F. Hlawatsch and G. F. Bourdeaux-Bartels, "Linear and quadratic time-frequency signal representations," *IEEE Signal Processing Mag.*, vol. 9, pp. 21–67, Apr. 1992.
- [5] H. M. Ozaktas, B. Barshan, and D. Mendlovic, "Convolution and filtering in fractional Fourier domain," *Opt. Rev.*, vol. 1, pp. 15–16, 1994.
- [6] H. M. Ozaktas, B. Barshan, D. Mendlovic, and L. Onural, "Convolution, filtering, and multiplexing in fractional Fourier domains and their relationship to chirp and wavelet transforms," *J. Opt. Soc. Amer. A*, vol. 11, pp. 547–559, Feb. 1994.
- [7] R. G. Dorsch, A. W. Lohmann, Y. Bitran, and D. Mendlovic, "Chirp filtering in the fractional Fourier domain," *Appl. Opt.*, vol. 33, pp. 7599–7602, 1994.
- [8] A. W. Lohmann and B. H. Soffer, "Relationships between the Radon–Wigner and fractional Fourier transforms," *J. Opt. Soc. Amer. A*, vol. 11, pp. 1798–1801, June 1994.
- [9] L. B. Almeida, "The fractional Fourier transform and time-frequency representation," *IEEE Trans. Signal Processing*, vol. 42, pp. 3084–3091, Nov. 1994.
- [10] D. Mendlovic, H. M. Ozaktas, and A. W. Lohmann, "Fractional correlation," *Appl. Opt.*, vol. 34, pp. 303–309, Jan. 1995.
- [11] H. M. Ozaktas, N. Erkaya, and M. A. Kutay, "Effect of fractional Fourier transformation on time-frequency distributions belonging to the Cohen class," *IEEE Signal Processing Lett.*, vol. 3, pp. 40–41, Feb. 1996.
- [12] D. Dragonman, "Fractional Wigner distribution function," *J. Opt. Soc. Amer. A*, vol. 13, pp. 474–478, Mar. 1996.
- [13] H. M. Ozaktas, "Fractional Fourier domains," *Signal Process.*, vol. 46, pp. 119–124, 1995.
- [14] D. Mendlovic and H. M. Ozaktas, "Fractional Fourier transformations and their optical implementation—I," *J. Opt. Soc. Amer. A*, vol. 10, pp. 1875–1881, 1993.
- [15] ———, "Fractional Fourier transformations and their optical implementation—II," *J. Opt. Soc. Amer. A*, vol. 10, pp. 2522–2531, 1993.
- [16] H. M. Ozaktas, O. Arikan, M. A. Kutay, and G. Bozdogan, "Digital computation of the fractional Fourier transform," *IEEE Trans. Signal Processing*, vol. 44, pp. 2141–2150, Sept. 1996.
- [17] B. Santhanam and J. H. McClellan, "The discrete rotational Fourier transform," *IEEE Trans. Signal Processing*, vol. 42, pp. 994–998, Apr. 1996.
- [18] G. Sansone, *Orthogonal Functions*. New York: Interscience, 1959.
- [19] B. A. Weisburn, T. W. Parks, and R. G. Shenoy, "Separation of transient signals," in *Proc. 6th IEEE DSP Workshop*, Oct. 1994, pp. 199–203.
- [20] B. W. Dickinson and K. Steiglitz, "Eigenvectors and functions of the discrete Fourier transform," *IEEE Trans. Acoust., Speech, Signal Processing*, vol. ASSP-30, pp. 25–31, Feb. 1982.
- [21] J. H. McClellan and T. W. Parks, "Eigenvalue and eigenvector decomposition of the discrete Fourier transform," *IEEE Trans. Audio Electroacoust.*, vol. AU-20, pp. 66–74, Mar. 1972.
- [22] G. Cincotti, F. Gori, and M. Santarsiero, "Generalized self-Fourier functions," *J. Phys.*, vol. 25, pp. 1191–1194, 1992.
- [23] A. V. Oppenheim, *Discrete-Time Signal Processing*. Englewood Cliffs, NJ: Prentice-Hall, 1989.
- [24] S. C. Pei and M. H. Yeh, "Discrete fractional Fourier transform," in *Proc. IEEE Int. Symp. Circuits Syst.*, May 1996, pp. 536–539.
- [25] ———, "Improved discrete fractional Fourier transform," *Opt. Lett.*, vol. 22, pp. 1047–1049, July 15, 1997.
- [26] ———, "Two dimensional discrete fractional Fourier transform," *Signal Process.*, vol. 67, pp. 99–108, 1998.
- [27] S. C. Pei, C.-C. Tseng, M.-H. Yeh, and J. J. Shyu, "Discrete fractional Hartley and Fourier transforms," *IEEE Trans. Circuits Syst. II*, vol. 45, pp. 665–675, 1998.
- [28] P. M. Morse and H. Feshbach, *Methods of Theoretical Physics*. New York: McGraw-Hill, 1953, p. 1416.
- [29] S. H. Friedberg, A. J. Insel, and L. E. Spence, *Linear Algebra*. Englewood Cliffs, NJ: Prentice-Hall, 1989.
- [30] G. H. Golub and C. F. Van Loan, *Matrix Computations*. Baltimore, MD: Johns Hopkins Univ. Press, 1989.
- [31] O. Arikan, M. A. Kutay, H. M. Ozaktas, and O. K. Aadamir, "The discrete fractional Fourier transform," in *Proc. IEEE Int. Symp. Time-Freq. Time-Scale Anal.*, June 1996, pp. 205–207.



Soo-Chang Pei (SM'89) was born in Soo-Auo, Taiwan, R.O.C., in 1949. He received the B.S.E.E. degree from the National Taiwan University (NTU), Taipei, in 1970 and the M.S.E.E. and Ph.D. degrees from the University of California, Santa Barbara (UCSB), in 1972 and 1975, respectively.

He was an Engineering Officer in the Chinese Navy Shipyard from 1970 to 1971. From 1971 to 1975, he was a Research Assistant at UCSB. He was a Professor and Chairman with the Electrical Engineering Department, Tatung Institute of Technology, Taipei, from 1981 to 1983. Presently, he is Professor and Chairman of the Electrical Engineering Department, NTU. His research interests include digital signal processing, image processing, optical information processing, and laser holography.

Dr. Pei is a Member of Eta Kappa Nu and the Optical Society of America.



Min-Hung Yeh was born in Taipei, Taiwan, R.O.C., in 1964. He received the B.S. degree in computer engineering from the National Chiao-Tung University, Hsinchu, Taiwan, in 1987. He then received the M.S. degree in computer science and information engineering in 1992 and the Ph.D. degree in electrical engineering in 1997, both from the National Taiwan University, Taipei.

He is currently an Assistant Professor with the Department of Computer Information Science, Tam-sui Oxford University College, Tam-sui, Taipei. His main research interests are in fractional Fourier transforms, time–frequency analysis, and wavelets.



Chien-Cheng Tseng (S'90–M'95) was born in Taipei, Taiwan, R.O.C., in 1965. He received the B.S. degree, with honors, from the Tatung Institute of Technology, Taipei, in 1988, and the M.S. and Ph.D. degrees from the National Taiwan University, Taipei, in 1990 and 1995, respectively, all in electrical engineering.

From 1995 to 1997, he was an Associate Research Engineer at Telecommunication Laboratories, Chunghwa Telecom Company, Ltd., Taoyuan, Taiwan. From 1997 to 1998, he was an Assistant Professor of the Department of Electronics Engineering, Hwa Hsia College of Technology and Commerce, Taipei. He is currently an Assistant Professor with the Department of Computer and Communication Engineering, National Kaohsiung First University of Science and Technology, Taipei. His research interests include digital signal processing, pattern recognition, and electronic commerce.